Bull. Mater. Sci. (2023)46:60
https://doi.org/10.1007/s12034-023-02903-9

Role of temperature and Ar flow on the uniformity of epitaxial graphene grown on SiC

ZHENZHEN ZHANG[1,†], DONGXUN YANG[1,†], GANG DONG[1], RUI LI[1], YI ZHANG[1], RAMIRO MORO[1], YANQING MA[1,2] and LEI MA[1,*]

[1] Tianjin International Center for Nanoparticles and Nanosystems, Tianjin University, Tianjin 300072, China
[2] State Laboratory of Precision Measuring Technology and Instruments, Tianjin University, Tianjin 300072, China
*Author for correspondence (lei.ma@tju.edu.cn)

[†] These authors have contributed equally to this study.

MS received 16 September 2022; accepted 4 December 2022

Abstract. Finite element methods based numerical simulations and experiments are conducted to systematically investigate the influence of temperature distribution and working gas flow to the growth of epitaxial graphene on SiC. It demonstrates the key role of temperature uniformity on the sample, which determines the coverage rate and quality of the grown graphene, as well as Ar flow for regulating the silicon partial vapour pressure. An optimized crucible was designed accordingly, which is successfully applied to prepare high coverage epitaxial graphene on the (0001) facet of SiC with great uniformity. Those insights might benefit the large-area high-quality epi-graphene growth for future industrial applications.

Keywords. Epitaxial graphene; graphite crucible; Ar gas flow rate; SiC.

1. Introduction

Graphene is a two-dimensional material with a honeycomb lattice formed by carbon atoms [1, 2]. In the past decades, great attention has been paid to its extraordinary electrical [2, 3], optical [4, 5] and mechanical properties [6] as well as the broad spectrum of its potential applications, including gas sensors [7], field-effect transistors (GFET) [8] and integrated circuits [9]. However, one of the most critical prerequisites for realizing those applications is the uniform large-scale growth of graphene on an insulating substrate [10]. In 2004, based on previously reported methods [11, 12], de Heer's group [2] proposed an improved epitaxial approach for graphene growth directly on silicon carbide (SiC) at moderate vacuum conditions with controlled background gas [13]. Many other methods have been used to study the growth of graphene, such as polymer-assisted sublimation growth [14], growth in different environments [15], etc. Specifically, epi-graphene refers to the epitaxially grown graphene on the silicon-terminated face (0001) of 4H and 6H SiC. In that approach, during the heating process, silicon atoms on the surface of SiC after chemical mechanical polishing are sublimated, and the remaining carbon atoms reconstruct to form graphene [11, 16, 17]. Since epi-graphene is directly grown on the semiconducting/semi-insulating substrate, it ultimately avoids defects and contamination that could occur during the graphene transfer process [18].

Graphene grown with an original crucible is non-uniform, as shown in supplementary figure S1d. Raman data are shown in supplementary table S1. The simulation results in supplementary figure S1c show that the temperature difference on SiC inside the crucible is as high as 20°C. The low temperature region grows monolayer graphene, and the high temperature region grows multilayer graphene. The uniformity of temperature and gas flow field largely depends on the structure of the graphite crucible, which is used as the heating container for SiC wafers [10, 19]. Understanding the mechanism of epi-graphene growth is crucial to optimize the crucible design for achieving the required uniformity. However, real-time measuring of the distribution of the temperature and gas flow inside the crucible remains challenging. Additionally, they are strongly coupled, so a little perturbation of one parameter will change the other. Hence, in this work, finite element methods were employed to elucidate this multiple-field process. Based on a systematic study of the aforementioned process and a series of comprehensive optimization

Supplementary Information: The online version contains supplementary material at https://doi.org/10.1007/s12034-023-02903-9.

Published online: 27 March 2023

procedures of the growth parameters, a new graphene growth crucible was designed. It realized full coverage and uniform graphene growth on SiC.

2. Experimental

The graphite crucible constructed in this work is shown in supplementary figure S2, and the geometry of the SiC wafer, its influence on gas dynamics, the coupling between the gas flow and the temperature distribution were considered. It consists of a top cover and a base with a rectangular groove instead of the traditional one-body cylindrical structure. At the bottom of the groove, there is another embedded shallow groove for placing the SiC sample. Two holes are drilled in the front and back of the rectangular groove as gas channels. In the experiment, the heater of EASYHEAT LI 8310 is adopted, the parameters of the heater are shown in supplementary table S2.

For growing epi-graphene, a SiC wafer is cleaned by a three-step ultrasonic process in which acetone, ethanol and deionized water are used sequentially. Then the wafer is placed on the shallow groove of the crucible with the Si-terminated face upwards. The crucible is put into a quartz tube and positioned in the centre of the induction coil. Before growth, the crucible is pre-heated inside high vacuum to eliminate water and other impurities. For comparison, epi-graphene was grown in two conditions: (1) with Ar flow at 1 atmosphere, and (2) inside high vacuum (10^{-6} mBar). In the former case, after pumping out the air from the quartz tube and completing the degassing at 850°C, the process was immediately followed by filling up with Ar and rapidly heating the system to the target temperature for epi-graphene growth.

In general, the growth process can be divided into four stages, which are represented as the temperature curve in supplementary figure S3. In the first stage (degassing), the crucible is heated up to 850°C for 30 s and maintained for 1200 s to reduce the remaining water, oxygen, polymers and other impurities on the inner surface of the crucible and the substrate [20]. In the second stage, the temperature is raised up to 1200°C at a rate of 10°C s^{-1} then kept for 1200 s. At this stage, step flow occurs on the SiC surface. In the third stage, the graphene growth happens after raising the temperature to 1590°C at a rate of 10°C s^{-1} and then kept for 2400 s. Finally, the induction furnace is shut down at the end of the third stage, and the sample is cooled down to room temperature naturally.

To study the influence of temperature and Ar flow on graphene uniformity and optimize the design of the crucible, numerical simulations of temperature and gas flow field in and out the crucible were carried out through finite element methods by using COMSOL Multiphysics. The model includes the graphite crucible with SiC wafer inside, the quartz tube and the water-cooled induction copper coil, as shown in supplementary figure S4. The critical parameters of the model are listed in supplementary table S2. The material types of each part in the model are listed in supplementary table S3.

The physical fields considered in the simulation are the flow field of Ar, the RF electromagnetic field produced by the coil, the inducted electric field in the crucible and the temperature field. The couplings between temperature field and the gas flow field were taken into account through iterations embedded in the software. The mesh sizes vary according to the components sizes to guarantee the accuracy with rational use of the computational resource.

3. Results and discussion

3.1 *Electromagnetic heating process*

The simulation of magnetic flux density is shown in supplementary figure S5a, and the induced current density is shown in supplementary figure S5b. The magnetic flux is concentrated in the middle of the coil, which is generated by RF current source. However, the magnetic field is weak inside due to the shielding effect caused by the induced current in the crucible. This current also produces Joule heating to the crucible to reach a temperature of over a thousand degrees Celsius within a few seconds.

To maximise the load power and achieve the homogeneity of the crucible heating, the correct selection of the geometry of the crucible relative to the dimensions of the inductor for good impedance match is necessary and important. The dimensions of the inductor are shown in supplementary figure S6. To obtain an optimized design regarding the highest temperature uniformity and impedance match, several cylindrical graphite crucibles with different geometric parameters, including length (L) and radius (R) of the bottom surfaces, are simulated under the same RF current and frequency. The results are shown in figure 1a and b. The increase of L will lead to the decrease of temperature of the crucible, while the temperature will increase with the increase of R. Both the increase of L and R will enlarge the temperature differences (Here, assuming all the RF power input is converted into heat). Figure 1c and d shows the temperature dependence on crucible volume and the ratio L/R, which indicates that the highest temperature appears at L/R equal to 3. When keeping the volume of the crucible as a constant, the minimum temperature difference is obtained at the L/R ratio of 2, it demonstrates that the temperature of this size crucible is uniform. As shown in figure 1e, with the lengthened crucible, the temperature rises and then drops. When the crucible length ranges from 14 to 18 mm, the temperature is relatively high, which indicates the best impedance match between the RF generator and the load. In our final design, the chosen length of the crucible is 17 mm. L/R is between 2 and 3, the crucible and the RF power supply output impedance match well; meanwhile, the temperature difference is relatively

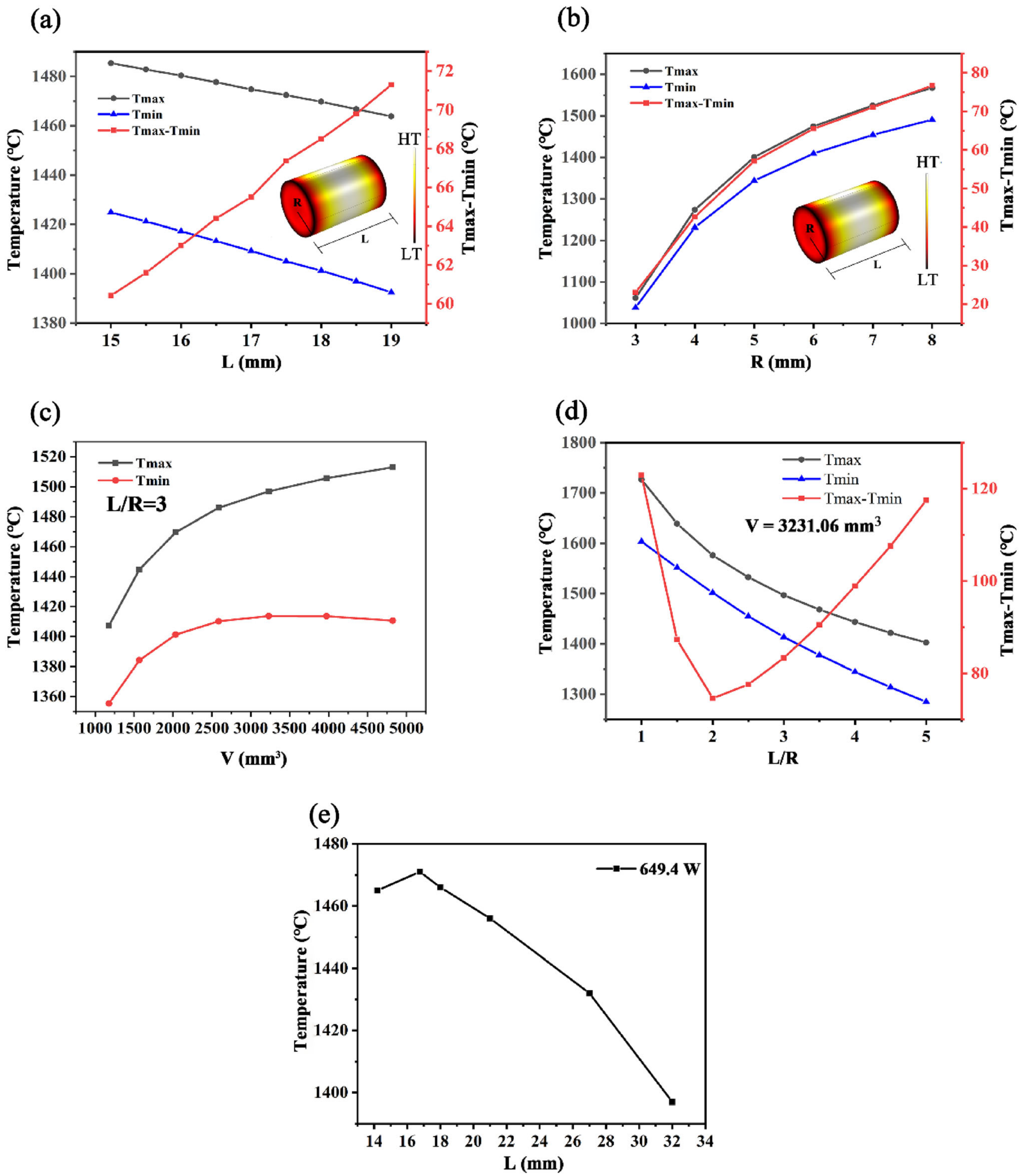

Figure 1. The calculated maximum and minimum temperatures inside the crucible with different geometric parameters: (**a**) at $R = 6$ mm, (**b**) at $L = 17$ mm, (**c**) at $L/R = 3$ and (**d**) at volume = 3231.1 mm^2. The illustrations in (**a**) and (**b**) are a schematic diagram of a crucible, showing the distribution of high temperature (HT) and low temperature (LT) of the crucible. (**e**) The actual experimentally measured temperature of crucible at different lengths with geometric parameters $R = 5.17$ mm (the input power is 649.4 W).

small, which ensures excellent temperature uniformity of the crucible and is benefit to uniform growth of graphene.

3.2 *Epi-graphene growth on SiC*

Step bunching occurs on the surface of the Si-face of SiC during annealing, which results from the minimization of surface free energy [21]. When cutting along the crystal plane, the surface will have a small miscut angle. After chemical mechanical polishing, the surface morphology of the Si-face presents an array of Si-C bilayer steps [22]. Due to the different atomic stacking order of the 4H-SiC, the surface energy between SiC bilayers steps is different, therefore, they flow at different rates [23]. When the temperature exceeds 1000°C, the surface oxides can be removed to avoid affecting the graphene growth [13, 24]. Due to the low coordination number of atoms at the edge, dislocations, defects and micropores, those structures are more unstable and tend to relax [25]. When wafer temperature is high enough, step flow start and will readily minimize the surface free energy [26], consequently releasing defects [25], improving the surface quality and enhancing its uniformity. Upon the same causes, SiC is preferentially decomposed from the edge of the steps, micropores and other sites with low atomic coordination number [25]. Furthermore, the Si atoms sublimate from the substrate leaving C atoms on the surface to form a C-rich layer and reconstruct to form graphene [13, 27].

3.2a *Epi-graphene growth in vacuum:* Graphene growth was directly carried out in vacuum to explore the dependence of graphene coverage rate on the inner temperature uniformity inside the crucible. A model of the coupled field of temperature and heat transfer speed was adopted. The temperature field and its *x*–*y* plane projection of the proposed crucible are shown in figure 2a and b. Although the temperature of the whole crucible ranges from 1462 to 1578°C, it is very uniform inside. The temperature distribution on the SiC surface is shown in figure 2c, where it varies from 1554.1 to 1554.9°C, which is within 1°C or less than 0.064% variation. Moreover, the temperature on the SiC surface along the *x* and *y* directions are presented in figure 2d, which indicates that the high-temperature areas are located at the two sides along the *y*-direction, and the low-temperature areas are along the *x*-direction. In vacuum, there are two main heat transfer channels: one is diffusion through solid–solid contact, which happens at the surface between SiC and the crucible and the other is radiation, which occurs between the crucible inner surface and the SiC, it can be quantified according to equation (1) as follows:

$$E = \left(\varepsilon_{\mathrm{SiC}} T^4_{\mathrm{SiC}} - \varepsilon_{\mathrm{crucible}} T^4_{\mathrm{crucible}}\right) \sigma S, \tag{1}$$

where E is the pure gain radiation power of the sample, $\varepsilon_{\mathrm{SiC}}$ and $\varepsilon_{\mathrm{crucible}}$ are the emissivity of the SiC and graphite crucible, respectively, σ is Stefan–Boltzmann constant and S the sample surface area.

Lateral force microscopy imaging of different locations (represented by the blue squares) in supplementary figure S7a are shown in supplementary figure S7b of the sample grown in vacuum. The coverage rate of the epi-graphene at each location ranges from 96.2 to 97.1%. The measured Raman spectra of ten points (black circles in supplementary figure S7a) are presented in supplementary figure S7c for layer number evaluation [28], which is summarized in supplementary table S4. It indicates that multilayer epi-graphene covers more than 96% of the surface. Owing to the minimal temperature differences over the surface, the coverage is rather uniform, but with variable number of layers due to the difficulty in controlling silicon evaporation in vacuum [29, 30] making it hard to grow uniform single-layer graphene on a large scale.

3.2b *Epi-graphene growth in Ar flow:* In order to unveil the process of epi-graphene growth in the presence of Ar flow, a non-isothermal flow field and temperature field coupled model was employed for simulation. The temperature distribution of crucible and tube are illustrated in figure 3a–c, respectively. Ar with a flow rate of 400 sccm is heated from room temperature to more than 1400°C when passing through the crucible. As shown in figure 3c, there is a 6.5°C temperature difference along the SiC varying from 1551 to 1557.5°C, which is larger than that in vacuum. However, all in all temperature distribution are similar as shown in figure 3d. The enlarged temperature difference on the SiC substrate is mainly due to the heating transfer effect of Ar.

The simulated Ar flow on the *x*–*y* plane above the SiC surface is shown in figure 3e. It clearly shows that the flow rate outside the crucible is 3 orders of magnitude higher than the flow rate inside the crucible. The density of the arrows represents the intensity and direction of the gas flow, as shown in figure 3f and g. The middle along the *x*-direction has higher flow rate than that area closes the wall of crucible. The direction of Ar flow inside the crucible is parallel to the *x*-direction. The flow rate distribution along *x* and *y* directions are displayed in figure 3h. In *x*-direction, the flow rate is between 0.85 and 0.95 mm s^{-1}. And, as expected, it is higher at the inlet and outlet than in the middle. In *y*-direction the flow rate ranges from 0.4 to 0.9 mm s^{-1}.

The blue squares in figure 4a and b show LFM images of epi-graphene grown in the Ar flow with the newly designed crucible. It demonstrates that the coverage rates of graphene were 93.9, 95.0, 95.9 and 94.9% in the areas (i), (ii), (iii) and (iv), respectively. There are three contrasts in LFM, the dark areas with large coverage are monolayer graphene. A few of darker areas are where the second layer of graphene has just begun to grow. The black circles in figure 4a and c show the locations where Raman spectra were taken. The shifts of 2D peak indicate the stress and stretch of graphene

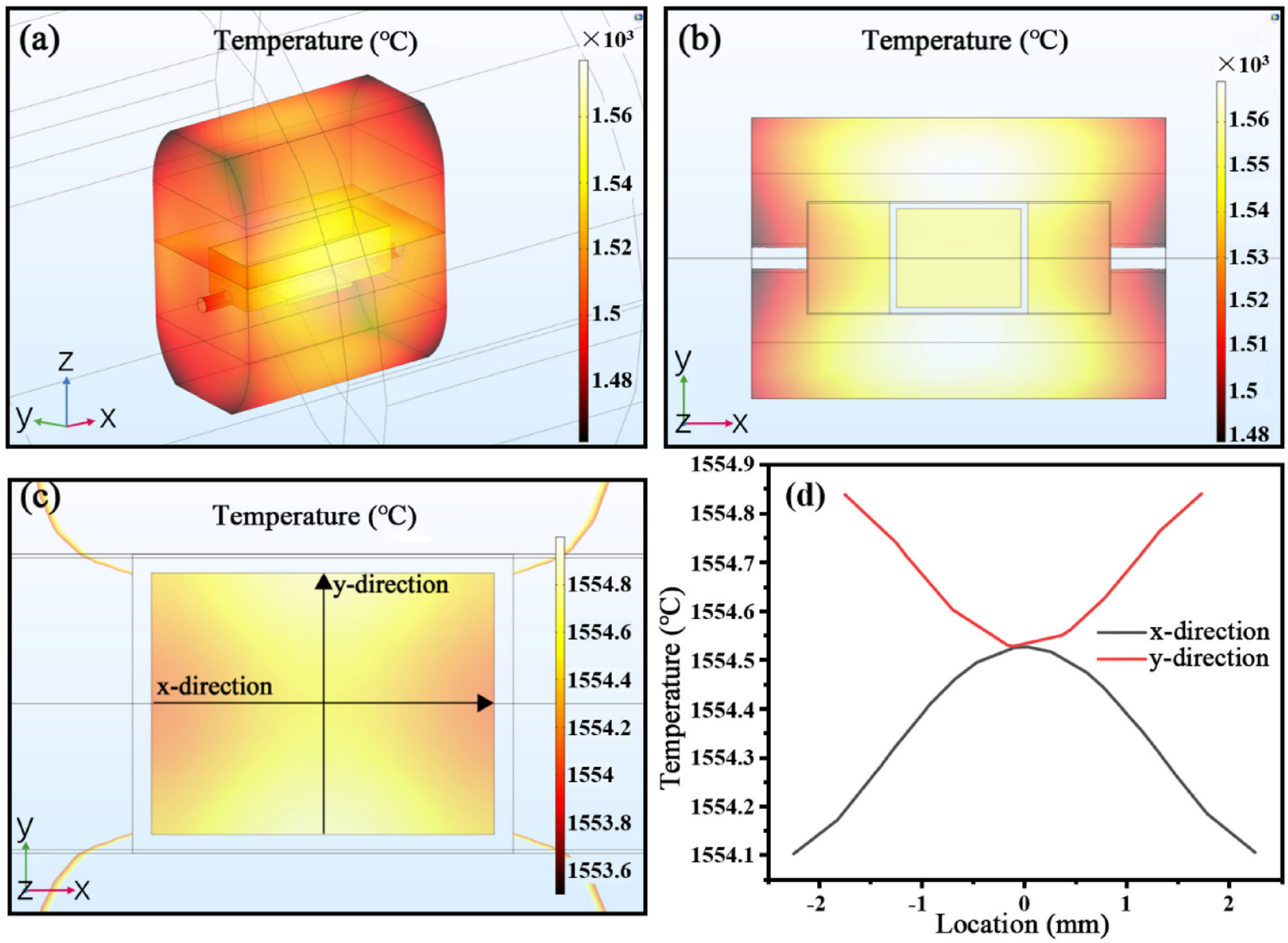

Figure 2. The calculated temperature distribution without Ar on (a) the surface of the crucible; (b) the x–y plane of the crucible; (c) the surface of SiC, (d) in x and y directions of the sample.

(Ar-2 and Ar-6 in figure 4c). Full-width at half-maximum (FWHM) of each measured 2D peak and the number of the graphene layers are listed in table 1. It demonstrates that the graphene grown under Ar flow has very high coverage, and uniformity. Apparently, the temperature difference increases compared to the case without Ar, but the presence of gas flow effectively diminishes the effect of temperature variation on the substrate to graphene growth.

The test results in figure 4 reflect the distribution of graphene thickness on SiC. Single-layer graphene covers a relatively large area on the sample surface, and most of it are grown near the outlet of crucible and four corners of the SiC substrate. The more samples have been characterized and relevant data are summarized in supplementary table S5. Supplementary figure S8 shows the LFM images of small scale (2 × 2 μm) monolayer graphene grown in argon. The measured Raman spectra show that out of ten randomly selected points eight of them indicate the feature of monolayer graphene, which can rationally be used for the monolayer graphene coverage evaluation about 80%. Moreover, bilayer graphene is mainly distributed near the inlet and the two sides along the y-direction. When Si atoms sublimate, they collide with the Ar atoms above, and some of them fall back. The Ar stream carries more Si vapour near the exit, which leads to the slower growth rate of that region and consequently the growth of monolayer graphene [31]. It also explains the preferential growth of single-layer graphene with Ar than in vacuum. Additionally, the existence of Ar will effectively smooth the density variation of silicon vapour above the SiC caused by temperature differences. Therefore, it further improves the uniformity of the grown graphene.

The preferential formation of bilayer graphene at the two sides in the y-direction can be attributed to the combined effect of high temperature and low Ar flow rate in those areas. Therefore, even though the temperature of the test point 1 (P1) is higher than the test point 4 (P4) by about 3.6°C, the graphene grown in the P1 region is still monolayer. Although the flow rate is low in P2 and P9, the temperatures there are the highest of the sample (the difference between P1 and P2 is about 2.9°C). The higher temperature leads to a faster growth rate of graphene, so

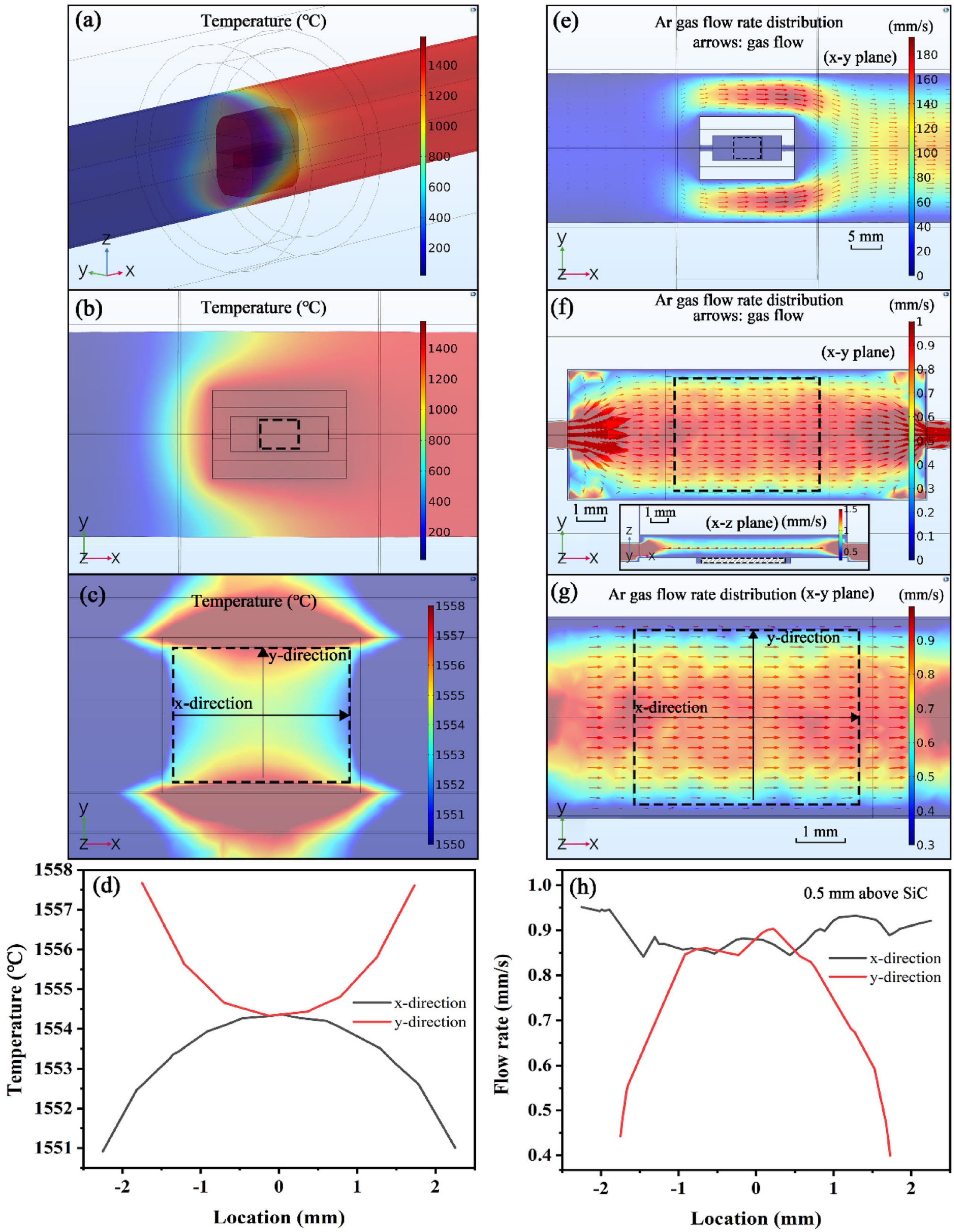

Figure 3. Calculated temperature distribution with Ar flow on (**a**) surface of the crucible and tube; (**b**) x–y plane of the crucible and tube; (**c**) surface of SiC. (**d**) Temperature distribution in x and y directions. Simulated flow rate distribution at (**e**) x–y plane of the crucible (**f**) above SiC. (**g**) Ar flow rate distribution on the SiC wafer. (**h**) Flow rate in the x and y directions.

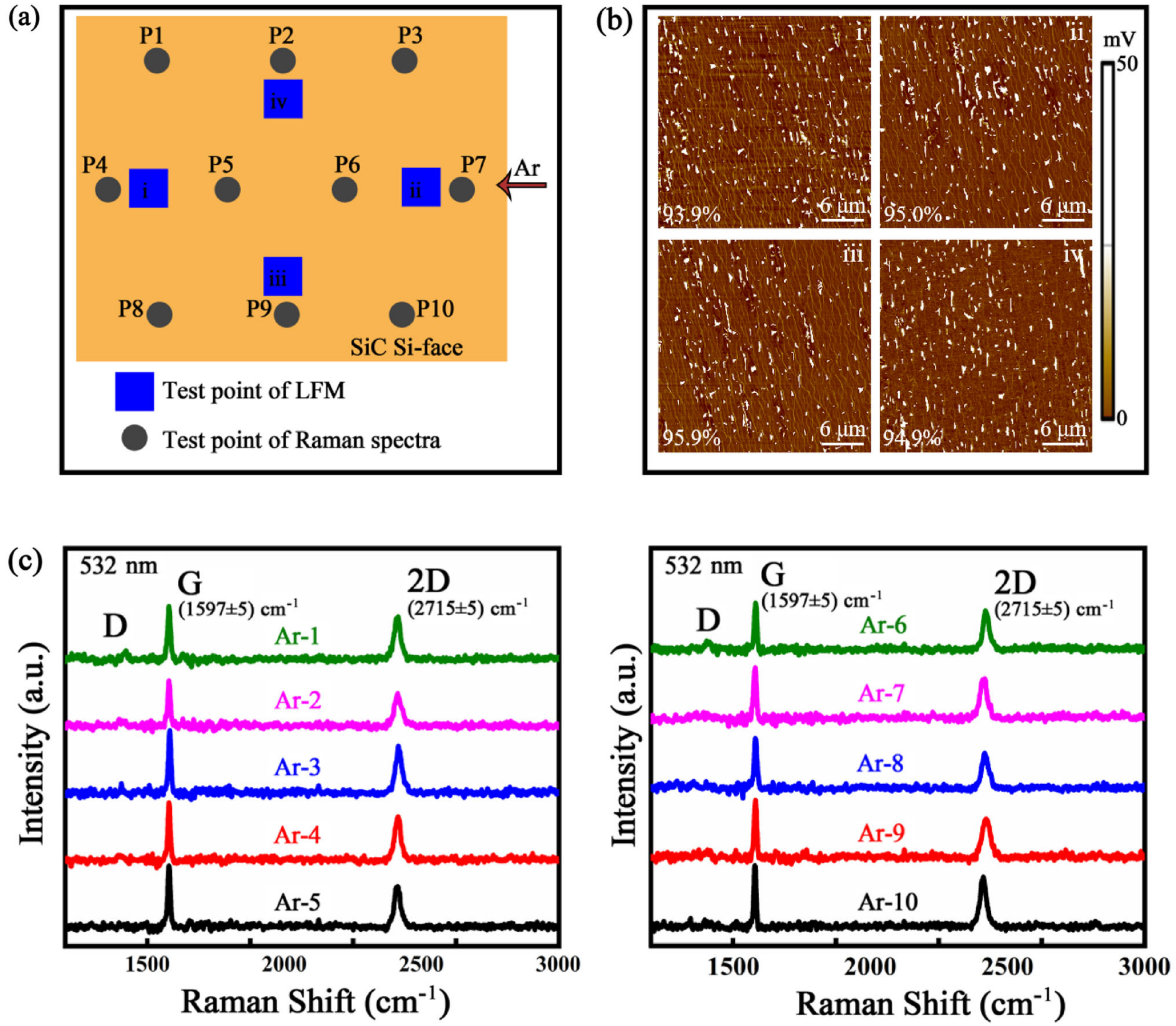

Figure 4. LFM images of epi-graphene on SiC grown in Ar flow at the tested points (i), (ii), (iii) and (iv), whose locations are indicated by blue squares in (**a**). (**b**) The coverage rates are (i) 93.9%, (ii) 95.0%, (iii) 95.9%, (iv) 94.9%. The area of LFM images is 30×30 μm^2. The black circles in (**a**) represent the tested points of the graphene for Raman spectra measuring. G peak is 1597 ± 5 cm^{-1} and 2D peak is 2715 ± 5 cm^{-1}. The 2D peak shifts due to the presence of stress. (**c**) Raman spectra (after subtracting the SiC signal) of each tested point on the epi-graphene grown in Ar atmosphere, where the spot size is 1 μm.

Table 1. FWHM of 2D peak in the measured Raman spectra at the tested points.

No.	FWHM of 2D peak (cm^{-1})	Layer	No.	FWHM of 2D peak (cm^{-1})	Layer
P1	38	1	P6	36	1
P2	49	1–2	P7	36	1
P3	36	1	P8	36	1
P4	40	1	P9	43	1–2
P5	40	1	P10	37	1

that it tends to generate bilayer graphene. Therefore, the key to realize large area and high uniform graphene growth is to fine tune the distribution of both temperature and gas flow rate inside the crucible. Here, changing the structure of the crucible has been proven as an effective approach to control the temperature and the Ar flow rate.

4. Conclusion

The dependence of epi-graphene growth on temperature and Ar flow rate distribution has been systematically studied through both experimental and numerical simulations. Especially, the finite elements based numerical methods were used for simulating the multi-field coupling problem. Therefore, the temperature and gas flow rate distributions are obtained simultaneously through active iterations. The measurements of LFM and Raman spectra confirm the correlation between the quality of epi-graphene grown on SiC, such as the uniformity, coverage rate and number of layers with the growing conditions. It unambiguously demonstrates the decisive role of temperature uniformity of the SiC surface on the uniformity and coverage rate of epi-graphene, where the Ar flow inhibits the graphene growth speed through changing the pressure of evaporated Si. Accordingly, a newly designed crucible achieves a high coverage of 94% in the optimized conditions with uniform graphene layers (the occupation of single-layer graphene is 80%), which we hope can contribute to the industrial application of epitaxial graphene.

Acknowledgements

This study was supported by the National Natural Science Foundation of China (No. 11774255) and the National Key R&D Program of China (No. 2020YFC2004602).

References

[1] Novoselov K S, Geim A K, Morozov S V, Jiang D, Katsnelson M I, Grigorieva I V *et al* 2005 *Nature* **438** 197
[2] de Heer W A, Berger C, Wu X, First P N, Conrad E H, Li X *et al* 2007 *Solid State Commun.* **143** 92
[3] Novoselov K S, Geim A K, Morozov S V, Jiang D, Zhang Y, Dubonos S V *et al* 2004 *Science* **306** 666
[4] Horng J, Balch H B, McGuire A F, Tsai H Z, Forrester P R, Crommie M F *et al* 2016 *Nat. Commun.* **7** 13704
[5] Ju L, Geng B, Horng J, Girit C, Martin M, Hao Z *et al* 2011 *Nat. Nanotechnol.* **6** 630
[6] Lin K, Li D, Song S, Ye Z, Jiang W and Qin Q H 2020 *Nanotechnology* **31** 195702
[7] Schedin F, Geim A K, Morozov S V, Hill E W, Blake P, Katsnelson M I *et al* 2007 *Nat. Mater.* **6** 652
[8] Cheli M, Michetti P and Iannaccone G 2010 *IEEE Trans. Electron Devices* **57** 1936
[9] Lin Y M, Valdes-Garcia A, Han S J, Farmer D B, Meric I, Sun Y *et al* 2011 *Science* **332** 1294
[10] Yazdi G, Iakimov T and Yakimova R 2016 *Crystals* **6** 53
[11] Van Bommel A J, Crombeen J E and Van Tooren A 1975 *Surf. Sci.* **48** 463
[12] Charrier A, Coati A, Argunova T, Thibaudau F, Garreau Y, Pinchaux R *et al* 2002 *J. Appl. Phys.* **92** 2479
[13] Berger C, Song Z M, Li T B, Li X B, Ogbazghi A Y, Feng R *et al* 2004 *J. Phys. Chem. B* **108** 19912
[14] Momeni Pakdehi D, Aprojanz J, Sinterhauf A, Pierz K, Kruskopf M, Willke P *et al* 2018 *ACS Appl. Mater. Interfaces* **10** 6039
[15] Kunc J, Rejhon M, Belas E, Dědič V, Moravec P and Franc J 2017 *Phys. Rev. Appl.* **8** 044011
[16] Forbeaux I, Themlin J M, Charrier A, Thibaudau F and Debever J M 2000 *Appl. Surf. Sci.* **162–163** 406
[17] Ji P, Zhang K, Zhang Z, Zhao M, Li R, Hao D *et al* 2022 *Mater. Sci. Semicond. Process.* **144** 106628
[18] Kaushik P D, Rodner M, Lakshmi G B V S, Ivanov I G, Greczynski G, Palisaitis J *et al* 2020 *Carbon* **157** 169
[19] Li R, Zhang K, Zhang Y, Zhang Z, Ji P, Shi C *et al* 2022 *Mater. Sci. Semicond. Process.* **149** 106896
[20] Kusunoki M, Rokkaku M and Suzuki T 1997 *Appl. Phys. Lett.* **71** 2620
[21] Kimoto T, Itoh A and Matsunami H 1995 *Appl. Phys. Lett.* **66** 3645
[22] Zhou Y, Pan G, Shi X, Gong H, Luo G and Gu Z 2014 *Surf. Coat. Technol.* **251** 48
[23] Yazdi G R, Vasiliauskas R, Iakimov T, Zakharov A, Syväjärvi M and Yakimova R 2013 *Carbon* **57** 477
[24] Bernhardt J, Nerding M, Starke U and Heinz K 1999 *Mater. Sci. Eng. B Adv. Funct. Solid State Mater.* **61–62** 207
[25] van der Berg N G, Malherbe J B, Botha A J and Friedland E 2012 *Appl. Surf. Sci.* **258** 5561
[26] Nishiguchi T, Ohshima S and Nishino S 2003 *Jpn. J. Appl. Phys.* **42** 1533
[27] Drowart J, De Maria G and Inghram M G 1958 *J. Chem. Phys.* **29** 1015
[28] Ni Z H, Chen W, Fan X F, Kuo J L, Yu T, Wee A T S *et al* 2008 *Phys. Rev. B* **77** 115416
[29] Emtsev K V, Bostwick A, Horn K, Jobst J, Kellogg G L, Ley L *et al* 2009 *Nat. Mater.* **8** 203
[30] Ohta T, El Gabaly F, Bostwick A, McChesney J L, Emtsev K V, Schmid A K *et al* 2008 *New J. Phys.* **10** 023034
[31] Yakimova R, Virojanadara C, Gogova D, Syväjärvi M, Siche D, Larsson K *et al* 2010 *Mater. Sci. Forum* **645–648** 565